



Contents lists available at ScienceDirect

Spectrochimica Acta Part A: Molecular and Biomolecular Spectroscopy

journal homepage: www.journals.elsevier.com/spectrochimica-acta-part-a-molecular-and-biomolecular-spectroscopy

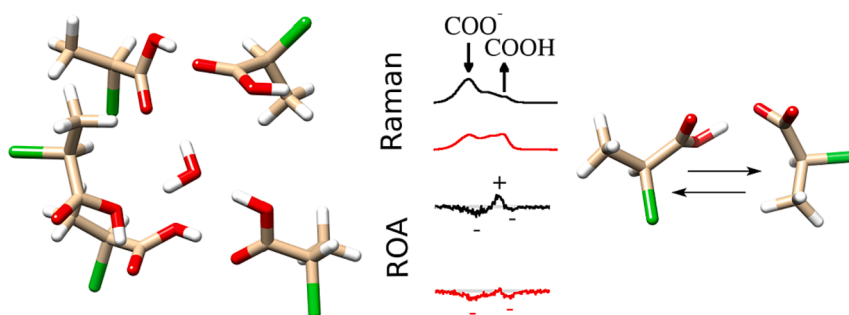
Conformations and hydration of halopropionic acids studied by molecular dynamics and Raman optical activity

Marie Berešová^a, Jiří Bufka^{a,b}, Martin Šafařík^a, Petr Bouř^a, Jaroslav Šebestík^{a,*}^a Institute of Organic Chemistry and Biochemistry, Academy of Sciences, Flemingovo náměstí 2, 16610 Prague 6, Czech Republic^b Department of Pediatrics, Faculty of Medicine in Pilsen, Faculty Hospital, Charles University in Prague, Alej Svobody 80, 323 00 Pilsen, Czech Republic

HIGHLIGHTS

- Traces of water in the sample can change the signs of ROA bands.
- This was explained by supramolecular organization of studied acids around water and changed acidobasic equilibria.
- Raman and ROA spectra of halogenated compounds were interpreted using MD/DFT.
- Esterification of the halo acids caused significant changes in vibrational spectra.

GRAPHICAL ABSTRACT



ARTICLE INFO

Keywords:

Chiral halocompounds
Raman optical activity (ROA)
Density functional theory (DFT)
Solvation effects

ABSTRACT

Chiral 2-halopropionic acids and their derivatives were synthesized and their properties studied computationally using Raman and Raman optical activity (ROA) spectroscopy. For neat acids present as liquids small amount of water led to significant changes in the spectra, resulting even to flipping of some ROA band signs. We find this interesting for the role water plays in interpretation of vibrational optical activity spectra of biomolecules. Analysis of the results shows that when the water is present, it can change ROA band signs due to the changes in acidobasic equilibrium. Corresponding esters without acidic hydrogens do not exhibit such effects.

1. Introduction

Prochiral or chiral 2-haloalkanecarboxylic acids and their esters serve as synthons for syntheses of chiral compounds and sophisticated

polymers. Especially bromoalkanoates play a crucial role in atom-transfer radical polymerization (ATRP) [1,2] and were used for syntheses of brush polymers. [3] Polymers containing 2-bromopropionates at the terminus were used for construction of shell cross-linked

Abbreviations: ACN, Acetonitrile; ATRP, Atom-transfer radical polymerisation; BRE, Ethyl 2-bromopropionate; BRK, 2-Bromopropionic acid; BRN, 2-Bromopropionate anion; CCT, Cartesian coordinate-based tensor transfer method; CID, Circular intensity difference; CLE, Ethyl 2-chloropropionate; CLK, 2-Chloropropionic acid; CLN, 2-Chloropropionate anion; CPCM, Conductor-like polarizable continuum model; DFT, Density functional theory; ESI, Electrospray ionization; FWHH, Full width (of a spectral peak) at half height; HF, Hartree Fock; IE, Ethyl 2-iodopropionate; IR, Infrared absorption; MD, Molecular dynamics; MS, Mass spectrometry; ROA, Raman optical activity; TFA, Trifluoroacetic acid; VCD, Vibrational circular dichroism.

* Corresponding author.

E-mail address: sebestik@uochb.cas.cz (J. Šebestík).

<https://doi.org/10.1016/j.saa.2024.123852>

Received 28 July 2023; Received in revised form 21 December 2023; Accepted 4 January 2024

Available online 8 January 2024

1386-1425/© 2024 Elsevier B.V. All rights reserved.

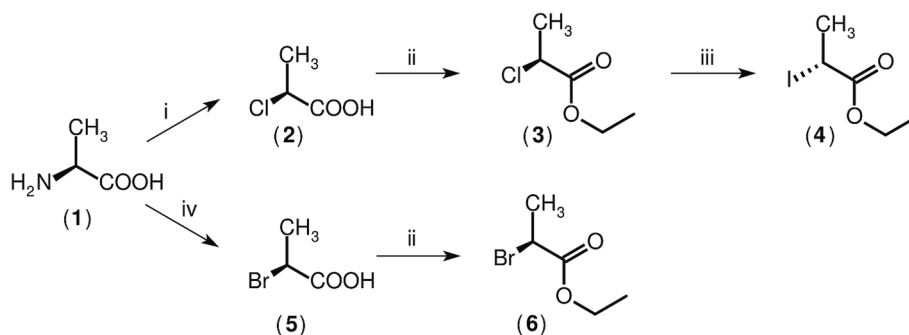


Fig. 1. Synthesis of studied compounds from L-alanine. Top: ethyl (2*R*)-iodopropionate (via Cl analogue), bottom: Br analogue, i) NaNO₂/HCl, ii) EtOH/PhH/H₂SO₄, iii) NaI/acetone, iv) NaNO₂/HBr/NaBr.

nanoparticles. [4] Ethyl bromopropionate was used as a precursor of juvenoids. [5,6] Moreover, the chiral halocompounds can play a role of pesticides, antimicrobial and antiviral drugs.

There is a limited number of methods allowing to study structure and properties of these compounds, but chiroptical spectroscopy appears very useful for this purpose. For example, optical rotation showed that interactions between methyl (2*R*)-chloropropionate and micelles were quite complex, and better understanding of molecular conformations is required. [7] Conformational tracking of ethyl propionate was achieved using theoretical methods and vibrational spectroscopies. [8] Chiral ethyl 2-bromopropionate was studied by circular dichroism [5,6] and chiral bromochlorofluoromethane was studied by Raman optical activity (ROA). [9] 2-Chloropropionic acid was investigated by combination of VCD and calculations, and the effects of strong and weak hydrogen bonding were discussed. [10] Hydrogen bonding of homochiral dimers of hydroxyesters was studied by ROA. [11] For ROA spectrum of methyl (2*S*)-chloropropionate the authors calculated structures of monomers and dimers of corresponding haloester. 4-Halo-2-azetidinones were studied using combination of ROA and calculations including the anharmonic effects. [12] A very detailed interpretation of anharmonic VOA spectra was achieved for relatively rigid 2-chloropropionitrile. [13]

Also for the 2-halopropionic acids and their esters studied here the ROA spectra provided useful information about chiral purity and molecular conformations. Surprisingly, tiny amount of water caused changes in ROA spectra of neat acids. We find this interesting because in common experiments water is taken as a solvent, while here it acts as an impurity. Observed spectral shapes could be interpreted using molecular dynamics and DFT simulations.

2. Material and methods

2.1. Synthesis

Briefly, *L*- and *D*-alanine were converted to (2*S*)- and (2*R*)-halopropionic acids, respectively. [14] Then, the acids were converted to ethyl (2*S*)- and (2*R*)-halopropionates by azeotropic esterification, using a mixture of benzene/ethanol and a small amount of sulfuric acid. [15]

Similar synthesis of iodoacids and iodoester was not possible due to reaction of iodides with nitrites, and Finkelstein's synthesis of the ester was carried out instead [16] (Fig. 1).

(2*S*)-Chloropropionic acid (2*S*) – Yield: 25.6 g, 53%. EA calcd. for C₃H₅ClO₂ (1.95% m/m H₂O): C, 32.55; H, 4.77. Found C, 32.52; H, 4.59. ESI HRMS (*m/z*): for [M–H][–] C₃H₄ClO₂ calcd. 106.99053; found 106.99028 (–2.33917 ppm). Specific rotation α₅₈₉ –17.6 (neat); lit. [14] –13.98 (neat). ¹H NMR (400 MHz, DMSO-*d*₆) δ 4.56 (q, *J* = 6.8 Hz, 1H, CHCl), 1.56 (d, *J* = 6.9 Hz, 3H, CH₃). ¹³C NMR (100 MHz, DMSO) δ 171.15 (COOH), 53.45 (CH), 21.52 (CH₃).

(2*R*)-Chloropropionic acid (2*R*) – Yield: 19 g, 49%. EA calcd. for C₃H₅ClO₂ (2.1% m/m H₂O): C, 32.50; H, 4.78. Found C, 32.48; H, 4.65.

ESI HRMS (*m/z*): for [M+H]⁺ C₃H₆ClO₂ calcd. 109.00508; found 109.00487 (–1.95422 ppm). Specific rotation α₅₈₉ +17.5 (neat); lit. [17] +17.39 (neat). ¹H NMR (400 MHz, DMSO-*d*₆) δ 13.23 (s br, 1H), 4.57 (q, *J* = 6.8 Hz, 1H, CHCl), 1.56 (d, *J* = 7.0 Hz, 3H, CH₃). ¹³C NMR (100 MHz, DMSO) δ 171.04 (COOH), 53.36 (CH), 21.44 (CH₃).

Ethyl (2*S*)-chloropropionate (3*S*) – Yield: 19.2 g, 61%. EA calcd. for C₅H₉O₂Cl: C, 43.97; H, 6.64. Found C, 43.96; H, 6.68. ESI HRMS (*m/z*): for [M+Na]⁺ C₅H₉O₂ClNa calcd. 159.01833; found 159.01776 (–3.56830 ppm). Specific rotation α₅₈₉ –20.28 (neat), lit. [18] α₅₈₉ –21.8. ¹H NMR (400 MHz, DMSO-*d*₆) δ 4.69 (q, *J* = 6.8 Hz, 1H, CHCl), 4.16 (q, *J* = 7.1 Hz, 2H, CH₂), 1.58 (d, *J* = 6.8 Hz, 3H, CH₃CHCl), 1.22 (t, *J* = 7.1 Hz, 3H, CH₃CH₂). ¹³C NMR (100 MHz, DMSO) δ 169.54 (COO), 61.59 (CH₂), 52.77 (CH), 21.19 (CH₃CHCl), 13.84 (CH₃CH₂).

Ethyl (2*R*)-chloropropionate (3*R*) – Yield: 19 g, 60%. EA calcd. for C₅H₉O₂Cl: C, 43.97; H, 6.64. Found C, 44.02; H, 6.55. ESI HRMS (*m/z*): for [M]⁺ C₅H₉O₂Cl calcd. 136.0291; found 136.0288 (–2.2 ppm). Specific rotation α₅₈₉ +19.8 (neat), lit. [19] α₅₇₉ +20.9 (neat). ¹H NMR (400 MHz, DMSO-*d*₆) δ 4.68 (q, *J* = 6.8 Hz, 1H, CHCl), 4.16 (q, *J* = 7.1 Hz, 2H, CH₂), 1.58 (d, *J* = 6.8 Hz, 3H, CH₃CHCl), 1.22 (t, *J* = 7.1 Hz, 3H, CH₃CH₂). ¹³C NMR (100 MHz, DMSO) δ 169.56 (COO), 61.61 (CH₂), 52.78 (CH), 21.20 (CH₃CHCl), 13.85 (CH₃CH₂).

Ethyl (2*R*)-iodopropionate (4*R*) – NaI (3.3 g, 22 mmol) was dried at 100 °C for 2 h at 40 mbar. After cooling down, ethyl ester 3*S* (3 g, 22 mmol) and acetone (15 ml) were added to the flask. Reaction mixture was stirred at 60 °C, solid was filtered off, and acetone was evaporated to dryness. Compound 4*R* was obtained by vacuum distillation (90 °C, 70 mbar). Yield 120 mg, 2%. ESI HRMS (*m/z*): for [M+H]⁺ C₅H₁₀O₂I calcd. 228.9726; found 228.9727 (0.4 ppm). Specific rotation α₅₈₉ –2.8 (neat), lit. [20] 1.88 (neat). ¹H NMR (400 MHz, CDCl₃) δ 4.47 (q, *J* = 7.0 Hz, 1H, CHI), 4.20 (qd, *J* = 7.1, 3.1 Hz, 2H, CH₂), 1.95 (d, *J* = 7.0 Hz, 3H, CH₃CHI), 1.28 (t, *J* = 7.1 Hz, 3H, CH₃CH₂).

(2*S*)-Bromopropionic acid (5*S*) – To a stirred cold solution of H–Ala–OH (20 g, 224 mmol), NaBr (62 g, 0.6 mol) in HBr (48%, 45 ml) and water (100 ml) at –10 °C, a solution of cold NaNO₂ (24.7 g, 358 mmol, in 50 ml water) was added dropwise within 3 h. The resulting reaction mixture was left stirring overnight. It was washed with Et₂O (3 × 200 ml). Organic layer was washed with brine (2 × 50 ml) and dried with Na₂SO₄. Residuum after evaporation (17 g) was vacuum distilled. The liquid fraction was collected at 105 °C using 16 mbar. Yield: 9 g, 26%. EA calcd. for C₃H₅BrO₂: C, 23.55; H, 3.29. Found C, 23.64; H, 3.25. ESI HRMS (*m/z*): for [M–H][–] C₃H₄BrO₂ calcd. 150.94002; found 150.94011 (0.62232 ppm). Specific rotation [α]_D²⁰ –26.90 (c 8.0156, MeOH); lit. [21] α₅₈₉ –27.2 (neat). ¹H NMR (400 MHz, CDCl₃) δ 10.83 (s, 1H, COOH), 4.40 (q, *J* = 7.0 Hz, 1H, CHBr), 1.85 (d, *J* = 6.9 Hz, 3H, CH₃). ¹³C NMR (100 MHz, CDCl₃) δ 176.40 (COOH), 39.47 (CH), 21.56 (CH₃).

(2*R*)-Bromopropionic acid (5*R*) – Yield: 17 g, 50%. EA calcd. for C₃H₅BrO₂: C, 23.55; H, 3.29. Found C, 23.43; H, 3.06. ESI HRMS (*m/z*): for [M–H][–] C₃H₄BrO₂ calcd. 150.94002; found 150.94016 (0.93953 ppm). Specific rotation α₅₈₉ +18.52 (neat); lit. [21] +27.2 (neat). ¹H

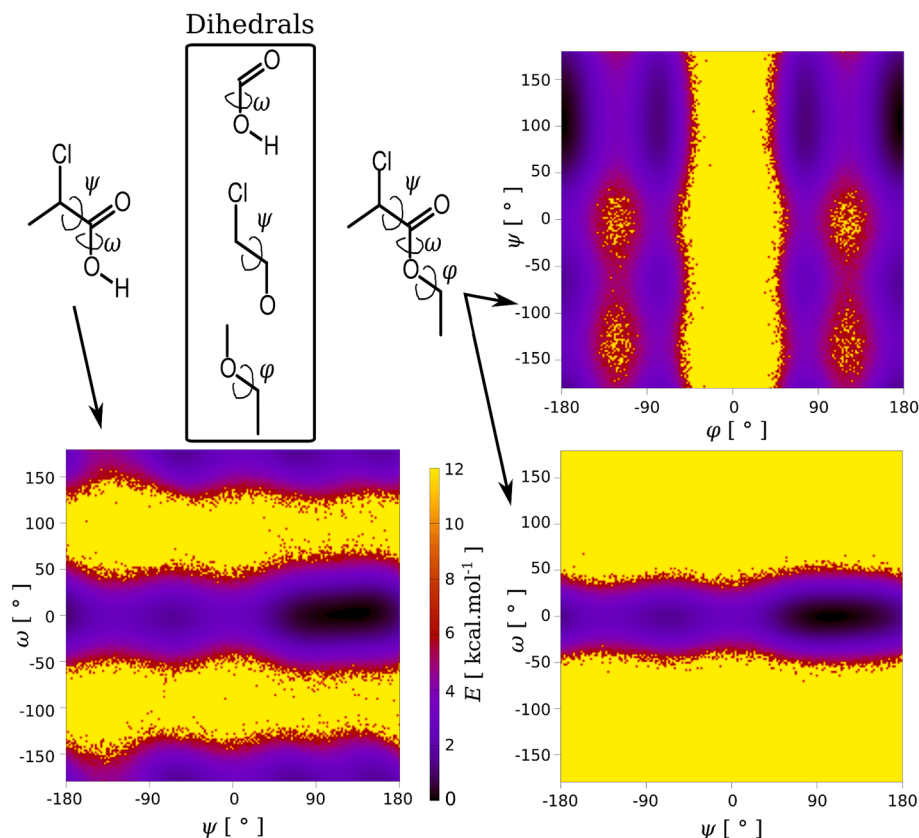


Fig. 2. Chloropropionic acid and ethyl chloropropionate, dependencies of the free energy on selected torsion angles, obtained from the MD simulations.

NMR (400 MHz, CDCl_3) δ 11.89 (s, 1H, COOH), 4.40 (q, $J = 7.0$ Hz, 1H, CHBr), 1.85 (d, $J = 7.0$ Hz, 3H, CH_3). **^{13}C NMR** (100 MHz, CDCl_3) δ 176.74 (COOH), 39.48 (CH), 21.52 (CH_3).

Ethyl (2S)-bromopropionate (**6s**) – Yield: 25 g, 60%. EA calcd. For $\text{C}_5\text{H}_9\text{O}_2\text{Br}$: C, 33.17; H, 5.01. Found C, 32.89; H, 4.99. **ESI HRMS** (m/z): for $[\text{M}+\text{Na}]^+$ $\text{C}_5\text{H}_9\text{O}_2\text{BrNa}$ calcd. 202.96781; found 202.96789 (0.39875 ppm). **Specific rotation** $[\alpha]_D^{20} -17.68$ (c 65.09, MeOH); lit. [22] -26.2 (c 1.00, CHCl_3). **^1H NMR** (400 MHz, CDCl_3) δ 4.35 (q, $J = 6.9$ Hz, 1H, CHBr), 4.22 (qd, $J = 7.1, 1.7$ Hz, 2H, CH_2), 1.81 (d, $J = 6.9$ Hz, 3H, CH_3CHBr), 1.29 (t, $J = 7.1$ Hz, 3H, CH_3CH_2). **^{13}C -APT NMR** (100 MHz, CDCl_3) δ 170.35 (COO), 62.10 (CH_2), 40.35 (CH), 21.77 (CH_3CHBr), 14.05 (CH_3CH_2).

Ethyl (2R)-bromopropionate (**6r**) – Yield: 7 g, 45%. EA calcd. For $\text{C}_5\text{H}_9\text{O}_2\text{Br}$: C, 33.17; H, 5.01. Found C, 33.11; H, 5.02. **ESI HRMS** (m/z): for $[\text{M}+\text{Na}]^+$ $\text{C}_5\text{H}_9\text{O}_2\text{BrNa}$ calcd. 202.96781; found 202.96753 (-1.40475 ppm). **Specific rotation** $[\alpha]_D^{20} +17.44$ (c 64.31, MeOH); lit. [5] $+23.9$ (c 0.43, CHCl_3). **^1H NMR** (400 MHz, CDCl_3) δ 4.33 (q, $J = 6.9$ Hz, 1H, CHBr), 4.20 (qd, $J = 7.2, 1.8$ Hz, 2H, CH_2), 1.79 (d, $J = 6.9$ Hz, 3H, CH_3CHBr), 1.27 (t, $J = 7.1$ Hz, 3H, CH_3CH_2). **^{13}C NMR** (100 MHz, CDCl_3) δ 170.28 (COO), 62.04 (CH_2), 40.30 (CH), 21.72 (CH_3CHBr), 14.00 (CH_3CH_2).

2.2. Raman and ROA spectra

Raman and ROA spectra of the halo derivatives acquired with a BioTools ChiralRAMAN-2X instrument (532 nm excitation wavelength, laser power 20 (iodine), 150 (bromine), or 400 (chlor) mW at source, 1.03–3.30 s illumination time per scan) were processed using homemade software. [23,24] Frequencies of the strongest Raman and ROA bands were labeled with the aid of a dedicated software. The samples were measured as neat liquids in 3×4 mm cell sealed with parafilm. If necessary, fluorescence was suppressed using subtraction of Akima polynomial.

2.3. Calculations

Starting geometries were optimized using the B3LYP/6-311++G** method as implemented in the Gaussian program. [25] With the aid of Gaussian, the atomic partial charges from electrostatic potential fitting were obtained and used in the molecular dynamic simulations performed in the Amber14 program. [26] A cube of $4 \times 4 \times 4$ nm³ volume was filled with investigated halo compounds, eventually some molecules of water or ions were added. In Amber, the geometry in the box was minimized, and free dynamics ran for 60–90 ns. Free energies as functions of the torsion angles were obtained from the trajectories (Fig. 2) and representative clusters selected for further computations.

The MD trajectories were analyzed using the cpptraj program of AmberTools, and a density-based clustering algorithm. Minimum number of points for a cluster was set to 10, distance cutoff for forming a cluster (ϵ) was set to 1.873 to 5.3 Å, sieve to frame options was on, and coordinate root-mean-squared deviation distance metric was used with sieve 5 for all atoms from the first solvation sphere of halocompounds or water (for selection of appropriate ϵ see our previous work [27]). This provided 52–228 representative, also used for further modeling.

Next, DFT calculations [28] were performed. The clusters were divided to dimers (cf. Scheme S1 in supplementary information), [29] their geometries partially optimized at the B3PW91/6-311++G** level with the CPCM(dichloroethane) solvent model and the GD3BJ dispersion correction. [30] For iodine, pseudopotential MWB46 was used. [31] The optimization used the vibrational normal mode coordinates, modes with frequencies smaller than 100 cm^{-1} were fixed. [32] For the optimized geometries vibrational spectra were calculated at the same level, using 532 nm excitation for Raman and ROA intensities. [33]

Alternatively, geometries of whole clusters were partially optimized and their harmonic force field calculated at the B3PW91/6-31G* level, using the same dispersion and solvent models. Vibrational parameters (polarizability tensors and force fields) of the dimers calculated at the

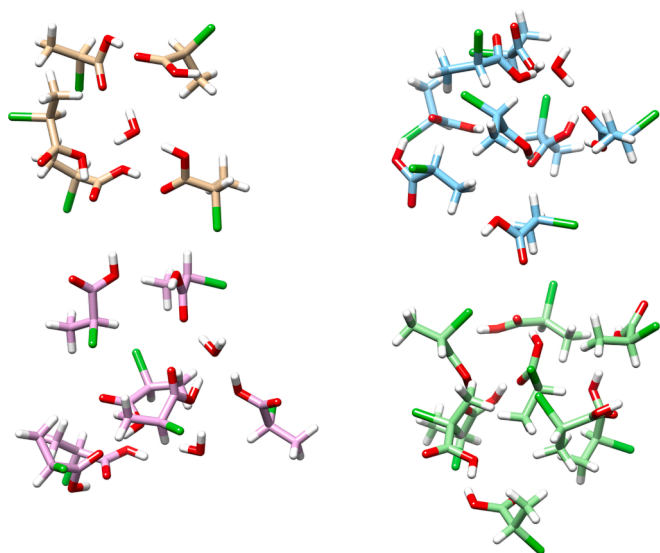


Fig. 3. Various model of chloropropionic acid solvation: H2O:CLK5, CLK8 + 1W, CLK8 + 2W, CLK8 (see text).

B3PW91/6-311++G** level were then transferred to the clusters, [34,35] and vibrational frequencies and spectral intensities calculated.

3. Results and discussions

3.1. Molecular conformers, selection of conformers/clusters for further calculations

The MD simulations suggest that the acids form *cis* and *trans* isomers, whereas the esters can exist solely in the *trans* isomers (Fig. 2, bottom plots, ω angle). The ψ angle supports three energy minima. In the case of the ester, there are also three local minima with respect to the φ angle. We have selected 3001 conformers using either loose or strict algorithm for the selection, to have a representative conformer distribution (Fig. S1). For the acid, the loose algorithm was used where the conformer can have energy equal or less than a threshold. For those

conformers, normal mode minimization somewhat modified the geometrical parameters, while for the strict algorithm original geometries were conserved more.

Since the chloropropionic acid (CLK) contained water, the influence of its presence on the spectra was modeled by box of $4 \times 4 \times 4 \text{ nm}^3$ volume containing 406 molecules of chloropropionic acid and 52 molecules of water. During such MD run, up to three molecules of water appeared in the first solvation sphere of chloropropionic acid (Fig. S2). Two types of clusters were selected for spectra simulations using cpptraj: with one water surrounded by 5 molecules of CLK, and with a CLK molecule surrounded by 8 other CLK molecules and three waters. For the second type, in a further selection molecules farther than 2.8 \AA from the central CLK were deleted. Examples of obtained clusters are shown in Fig. 3: H2O:CLK5 water in middle with 5 solvent molecules of CLK; CLK8 + 1W CLK in middle with up to 8 solvent CLK and one solvent of water; CLK8 + 2W CLK in middle with up to 8 solvent CLK and two solvent of water; and CLK8 CLK in middle with up to 8 solvent CLK. Combined model of solvation CLK8 + W consisted of all cluster from models CLK8 + 1W, CLK8 + 2W and CLK8.

3.2. Overview of experimental spectra

The most stable CLK and CLE derivatives were measured with a laser power of 400 mW. For the bromine analogues and the iodine ester 150 mW and 20 mW were used, respectively (Fig. 4). The higher power allowed for reduction of the illumination times. To be better visible at the same scale, the spectra of the bromine and iodine analogues were multiplied by the factor of 1.6 and 5000, respectively. At $\sim 1072 \text{ cm}^{-1}$, circular intensity differences (CID) for CLK, BRK, CLE, and BRE were 2.9×10^{-4} , 1.6×10^{-4} , 1.7×10^{-4} , and 1.2×10^{-4} , respectively. Spectra of enantiomeric pairs of CLK, BRK, CLE, and BRE are shown in supplementary materials (Figs. S3–S6). Spectral similarities and differences are discussed in section 3.4. Measurement of ethyl (2R)-iodopropionate ROA is discussed in section 3.5.

3.3. Calculations versus experiments

The simulated spectra of the chloro acid reproduced many experimental features (Fig. 5). The region of $600\text{--}1100 \text{ cm}^{-1}$ is best

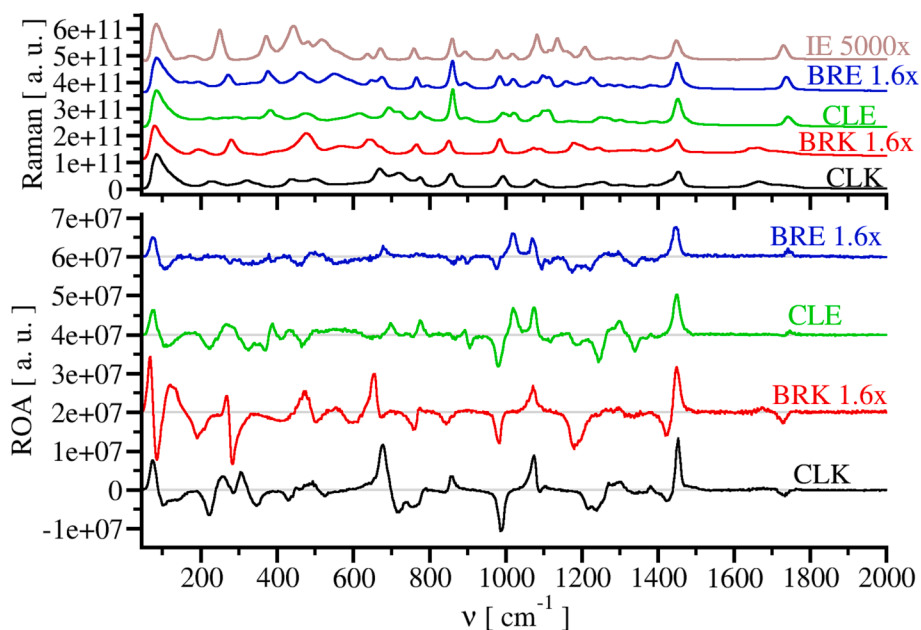


Fig. 4. Experimental spectra of (2S)-2-chloropropionic acid (CLK), (2S)-bromopropionic acid (BRK), ethyl (2S)-chloropropionate (CLE), ethyl (2S)-bromopropionate (BRE), and ethyl (2R)-iodopropionate (IE).

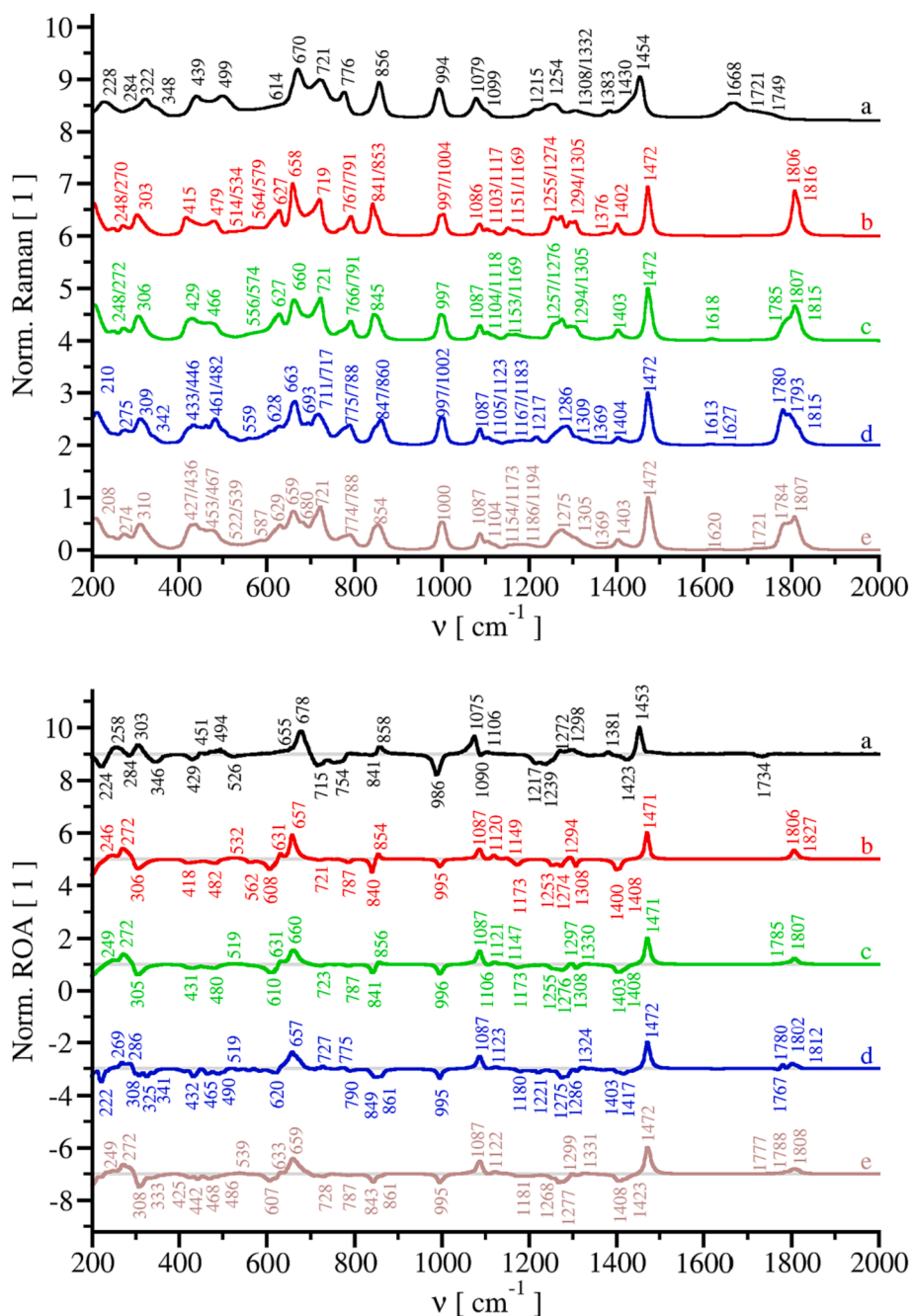


Fig. 5. Experimental (a) and calculated spectra (b-e) of (2S)-chloropropionic acid. The calculation models included b) monomers; c) dimers; d) H₂O:ClK5 clusters; and e) ClK8 + W clusters, averaged spectra from 79 ns. At 1079 cm⁻¹ (exp.) and ~1087 cm⁻¹ (calc.), CIDs were 2.9×10^{-4} , 5.2×10^{-4} , 5.8×10^{-4} , 5.1×10^{-4} , and 4.4×10^{-4} , respectively.

reproduced by the clusters with water molecule solvated by five CLKs. In experiment, the main carbonyl band (1668 cm⁻¹) is followed by sidebands at 1721 and 1749 cm⁻¹ of decreasing intensity. This is only reproduced by using the solvated water molecule (spectrum d). Interestingly, the carbonyl frequencies calculated for the neutral species are blue shifted by about 86 cm⁻¹, whereas those of anionic species are red shifted, by about 16 cm⁻¹ (Fig. 5 and S8). This inconsistency comes most probably from the used solvent model. At the carbonyl region all calculations predict ROA with a wrong sign, and spectra shape depends strongly on the solvation model (cf d and e; see also Fig. S7 in SI).

For ethyl (2S)-chloropropionate, Raman spectrum is well reproduced using all models; relative intensities of the bands at 374 cm⁻¹, 1298 cm⁻¹ and 1209 cm⁻¹ are slightly overestimated, while they are

underestimated at 880 cm⁻¹ and 1114 cm⁻¹ (Fig. 6, cf. Table S5 with band assignments). The ROA sign pattern is reasonably reproduced by all models as well, but relative intensities vary (Fig. 6). Unlike for the acid, the sign of the main carbonyl ROA peak 1747 cm⁻¹ (exp.) is calculated correctly. The small negative carbonyl peak at 1731 cm⁻¹ (exp.) is reproduced only when monomer spectra were averaged (b). Relative intensities of the -/+ bands at 981 and 1021 cm⁻¹ are underestimated by the calculations. Within 200–500 cm⁻¹ experimental ROA is best reproduced by the cluster calculation (d).

A worse agreement was achieved for the bromo derivative (Fig. S11 in SI, band assignment in Table S6), which might indicate inaccuracies of DFT for heavier elements.

Next we focused on the carbonyls in the experimental data for the

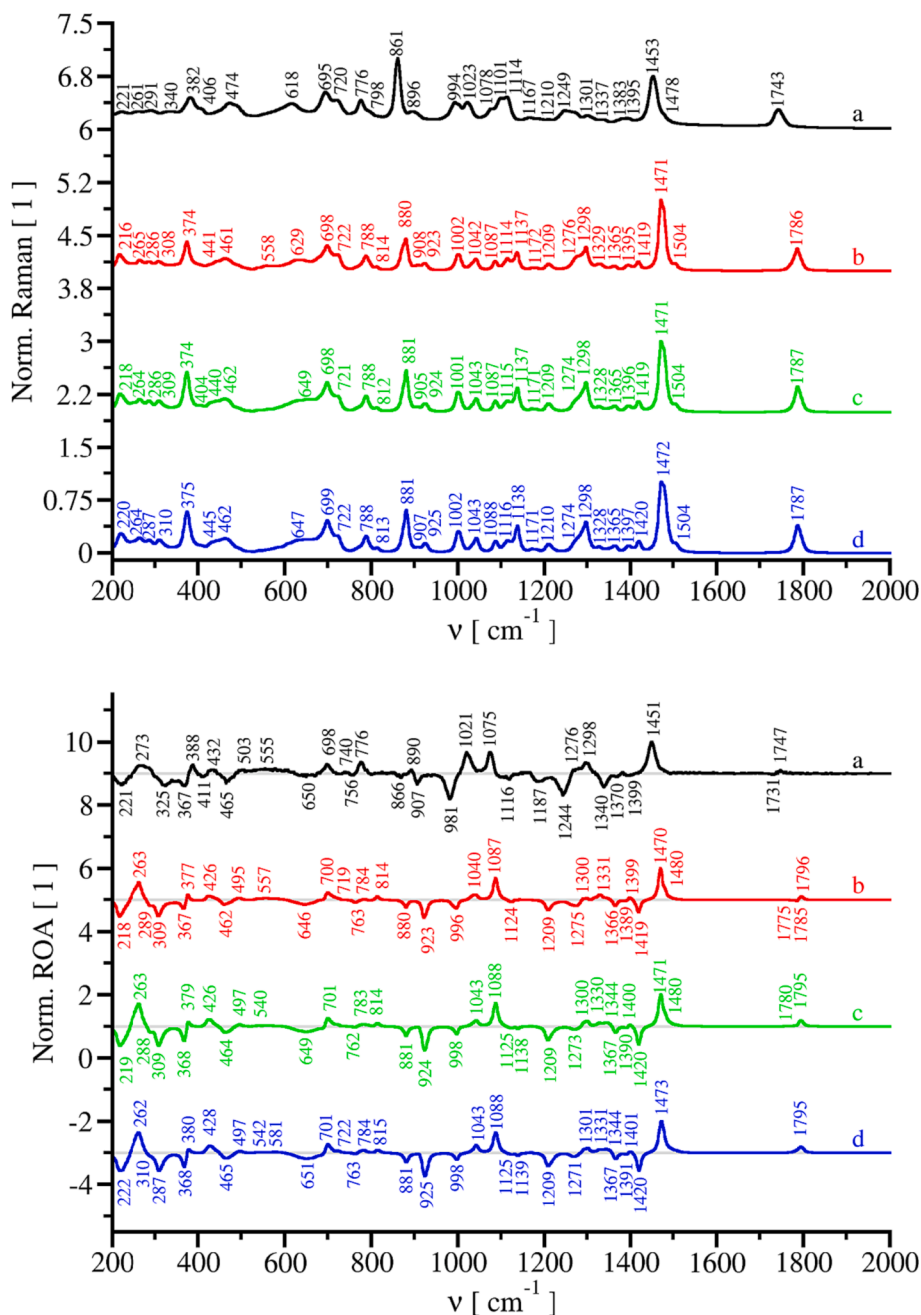


Fig. 6. Experimental (a) and calculated spectra (b-d) of ethyl (2S)-chloropropionate. b) monomers; c) dimers; and d) clusters. At 1078 cm^{-1} (exp.) and $\sim 1088\text{ cm}^{-1}$ (calc.), CIDs were 1.7×10^{-4} , 6.9×10^{-4} , 6.9×10^{-4} , and 5.7×10^{-4} , respectively.

chloro and bromoacids (Fig. 7). There is always a band at $\sim 1668\text{ cm}^{-1}$, followed by shoulders at ~ 1721 and $\sim 1749\text{ cm}^{-1}$. This can be explained by partial deprotonation of the acids and appearance of corresponding anion in presence of water. This is consistent with simulation of the solvated anion (Fig. S8 in SI). The anionic carbonyl is predicted to have opposite ROA sign than the acidic one, which would explain prediction of the wrong sign without consideration of the deprotonation (Fig. 5). In Fig. 7, we can also see that large parts of the spectra are for the two acids similar, suggesting similar conformations of both.

To further explore the effect of water, we treated the acid with CaCl_2 , to remove all water (Fig. 8 and S10). A short-term drying (150 min, b) led to the change of the prevalent ROA sign in the carbonyl region. However, drying for a longer time (one week, c) led to increase of fluorescence and deterioration of ROA signal. As expected, the drying also caused a decrease of the Raman COO^- signal at $\sim 1664\text{ cm}^{-1}$, and

increase of the COOH signals at ~ 1722 and 1745 cm^{-1} . In ROA, the positive band of carbonyls at 1728 cm^{-1} disappeared, and only negative bands at 1669 and 1754 cm^{-1} remained.

Due to the strong hygroscopicity of the halo acids, it was impossible to dry them completely (i.e. to achieve complete disappearance of the COO^- signal), either by CaCl_2 or P_4O_{10} . Usage of P_4O_{10} probably led to a formation of acid anhydrides and appearance of a new carbonyl band at 1831 cm^{-1} (Fig. S9 in SI). Thus CaCl_2 appeared as a more powerful and safer drying agent for the halogenated acids. Bromo acid is less hygroscopic than the chloro acid, and its drying with CaCl_2 led to a more visible decrease of the carboxylate signals. Similarly to chloro acid, the bromo acid gives opposite signs of ROA carbonyl bands in protonated and anionic forms (Fig. S10 in SI).

Similarly as for the chloro acid, for (2R)-bromopropionic acid the computational model can explain some but not all features in

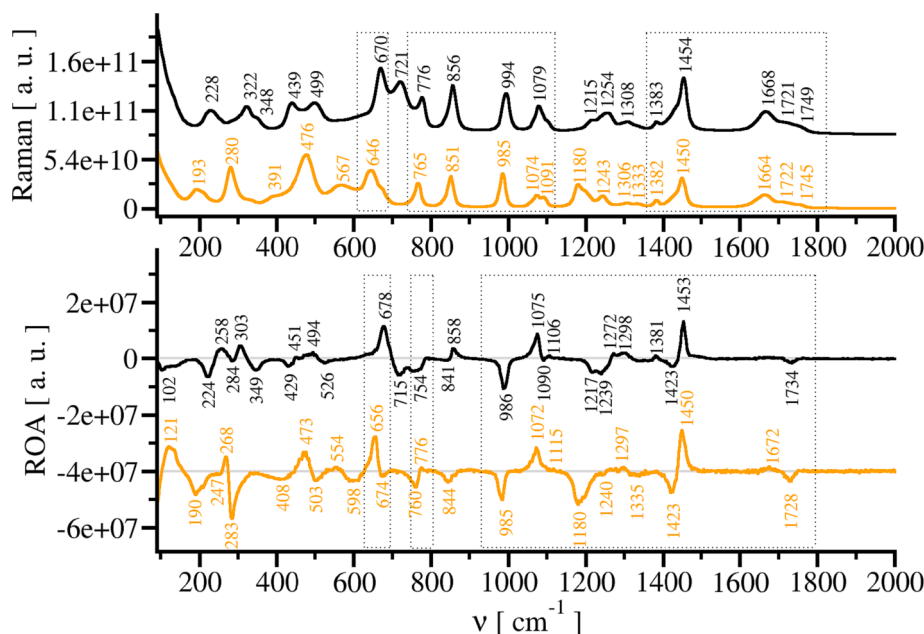


Fig. 7. Raman and ROA spectra of (2S)-chloropropionic acid (black) and (2S)-bromopropionic acid (yellow, 2x magnified). Relatively conserved regions are indicated by dotted rectangles. (For interpretation of the references to colour in this figure legend, the reader is referred to the web version of this article.)

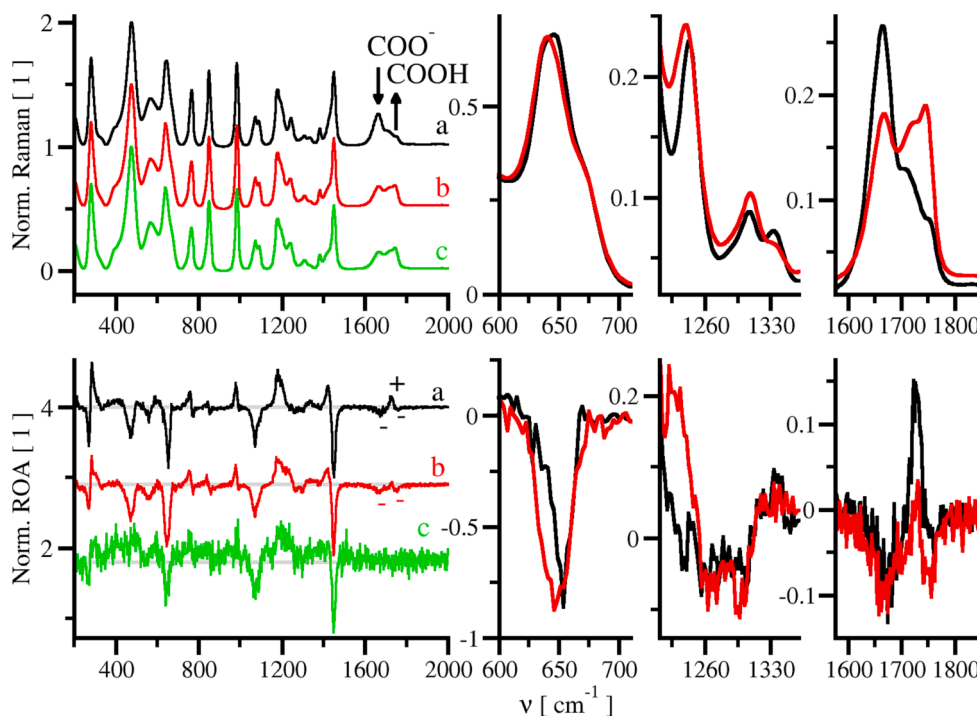


Fig. 8. Experimental spectra of original (a, "wet", black) and dried (b, c, red, green) (2R)-bromopropionic acid. The acid was dried in the presence of CaCl_2 for 150 min (b) or one week (c). Left - whole spectra, right - selected details. (For interpretation of the references to colour in this figure legend, the reader is referred to the web version of this article.)

experimental spectra. For instance, the carbonyl frequency of BRK is blue shifted by 78 cm^{-1} in neutral species and red shifted by 15 cm^{-1} in anionic species. In experimental spectrum obtained with higher concentration of the anion (Fig. S10, a), there are two negative peaks at 1672 and 1760 cm^{-1} , and a positive one at 1728 cm^{-1} . This corresponds to the calculated spectrum of the BRK + BRN dimer (Fig. S10, f) where there are two negative peaks at 1759 and 1803 cm^{-1} , and two overlapping positive at 1641 and 1649 cm^{-1} . When the concentration of

anionic species was reduced by the drying agent (Fig. S10, b), two negative peaks at 1669 and 1754 cm^{-1} appeared, which is again reproduced by the simulation of the BRK + BRK dimer (Fig. S10, e) with two negative peaks at 1782 and 1801 cm^{-1} . Below 1600 cm^{-1} most of ROA signs and relative intensities are well-reproduced by the computation, such as the couplet at 266 and 286 cm^{-1} or the negative peak at 656 cm^{-1} . For a better agreement, one perhaps has to consider more complicated mixture of acids, anions, water and oxonium ions,

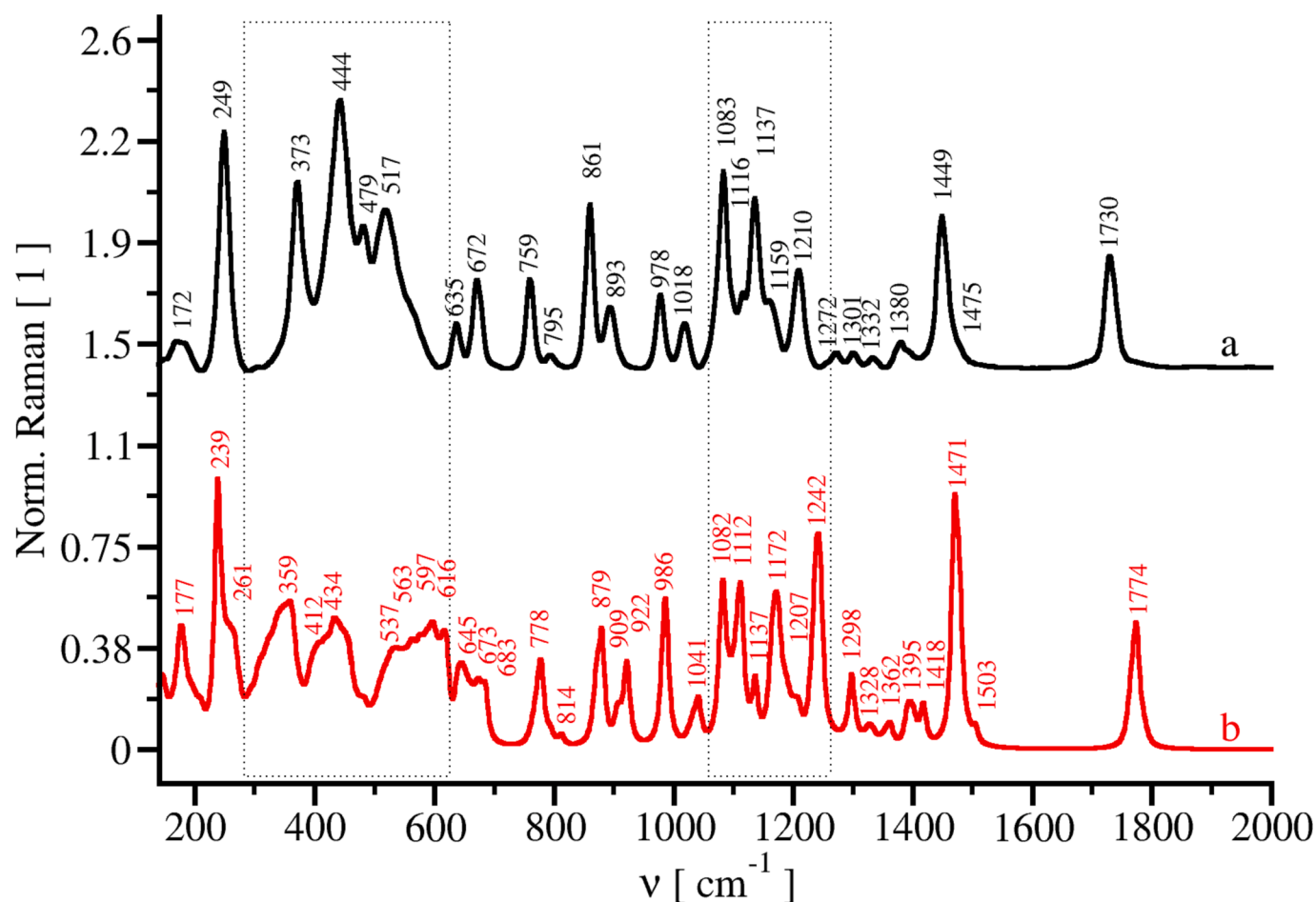


Fig. 9. Experimental (a) and calculated (b) Raman spectra of ethyl (2S/2R)-iodopropionate. Parts with significant differences between experiment and calculation are marked by dotted rectangles.

Table 1

Selected bands of studied compounds, frequencies in cm^{-1} , calculated values are averages from 3000 conformers.

Vibration	CLK		BRK		CLE		BRE		IE	
	Exp.	Calc.	Exp.	Calc.	Exp.	Calc.	Exp.	Calc.	Exp.	Calc.
$\nu(\text{C}=\text{O})$	1749, 1721, 1668	1806, 1652	1745, ~1722, 1664	~1812, 1800, 1651	1743	1786	1738	1781	1730	1774
$\delta(\text{HCH})$	1454	1472, 1468	1450	1471, 1466	1453	1471	1451	1471	1449	1471
$\delta(\text{HCX})$	1254	1274, 1255, 1242	~1195, 1180	~1235, 1205	1272, 1249, 1210	~1276, 1209	1225, 1205, 1159	1260, 1194	1210, 1137, 1083	1242, 1172, 1112
$\nu(\text{C}-\text{X})$,	721, 670	719, 658, 415, 678	646, 476	627, 450, 350, 626, 434, 348	720, 695, 618	722, 698, 629	675, 647, 552, 462, 376	685, 656, 568, 449, 366	672, 635, 517, 479, 444, 373	673, 645, 616, 597-537, 434, 359
$\delta(\text{C}_{\text{Me}}\text{CX})$	322	303, 305	280	271, 272	221	216	193	192	~172	177
$\delta(\text{C}=\text{O}\text{CX})$	-	-	-	-	382, 291	374, 308	273	271	249	~261, 239

Italic numbers relate to anion, ν - stretching, δ - bending.

which goes beyond the topic of the present study. As for the chloro ester, the ROA sign of bromo ester carbonyl is positive, in agreement with the calculation (Fig. S11 in SI).

We were not able to obtain experimental ROA spectra of ethyl (2R)-iodopropionate (see section 3.5), but we can compare the experiment

and simulation for the Raman spectrum (Fig. 9). There are some inconsistencies in region of $283\text{--}625\text{ cm}^{-1}$ containing modes such as $\nu(\text{C}-\text{I})$, $\delta(\text{CCI})$, $\delta(\text{CCO})$, $\delta(\text{CCC})$, $\tau(\text{CO})$ (see also Table S7 with detailed assignment). Other “problematic” region of iodo ester spectra of $1059\text{--}1270\text{ cm}^{-1}$ involves $\delta(\text{HCI})$ vibrations. Here, calculated intensities

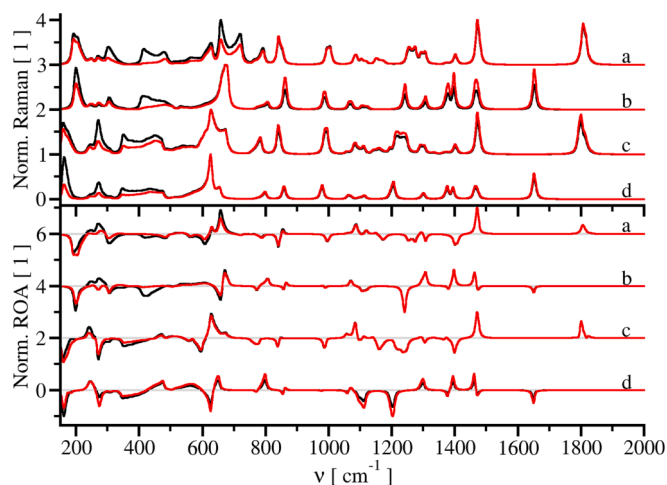


Fig. 10. Raman and ROA spectra of calculated monomeric acids and anions with (black) and without (red) halogen contributions, a) CLK; b) CLN; c) BRK; d) BRN. (For interpretation of the references to colour in this figure legend, the reader is referred to the web version of this article.)

at 1112, 1172 and 1242 cm^{-1} are much higher than corresponding experimental ones.

3.4. Spectral similarities/differences between chloro and bromo derivatives

In Fig. 7, we saw some quasi conserved regions in the spectra of chloro and bromo propionic acids, such as the $\nu(\text{C}=\text{O})$ vibrations at 1746 and 1667 cm^{-1} (see also Table 1). Other well preserved patterns include modes $\delta(\text{HCH})$ and $\delta(\text{HCC})$ at 1454 and 1427 cm^{-1} (chloro derivative), which frequencies differing by about 3 cm^{-1} between chloro and bromo derivatives. Obviously, bands related to the halogens change more, such as the strong negative ROA $\delta(\text{HCX})$ peak moved from 1220 cm^{-1} (Cl) to 1179 cm^{-1} (Br). The more polarizable bromine provides stronger ROA (if normalized to laser power and accumulation time). ROA bands involving $\delta(\text{HCC})$, $\nu(\text{C}-\text{C})$, $\delta(\text{HOC})$, and $\tau(\text{CO})$ around 860

cm^{-1} change signs from positive to negative at chloro and bromo derivatives, respectively. The distinct $\nu(\text{C}-\text{Cl})$ vibration at 721 cm^{-1} is unique for the chloro derivative. It was previously shown that position of the $\nu(\text{C}-\text{Cl})$ vibration of PVC can vary depending on mutual orientation of the chlorine containing units, between 614 and 704 cm^{-1} . [36] From the calculations (Fig. S12 in SI), we see that $\nu(\text{C}-\text{Cl})$ also contributes to vibrations within 408–417, 424–463, 650–683, and 717–725 cm^{-1} .

To better understand influence of the halogen atoms on the spectra, we calculated them with and without contributions of the polarizability derivatives related to the halogen (Fig. 10). Vibrations containing $\delta(\text{HCX})$ movement are especially affected in Raman intensities. On the other hand, $\nu(\text{C}-\text{Cl})$ and $\delta(\text{C}_{\text{Me}}\text{CCl})$ modes loose only ca. 50% of Raman intensity after the chlorine deletion. Similar effect is also observed for the $\nu(\text{C}-\text{Br})$ and $\delta(\text{C}_{\text{Me}}\text{CBr})$ modes. In case of the chloropropionate, the chlorine atom also significantly contributes to Raman intensities of all vibrations between 800 and 2000 cm^{-1} .

Further analysis of changes of internal coordinates under vibrational motions revealed that the acid ethylation causes reordering of the $\delta(\text{C}_{\text{Me}}\text{CX})$ and $\delta(\text{C}_{\text{C}=\text{O}}\text{CX})$ vibrations in corresponding acids and esters (Figs. S12–S16 in SI). For esters, the $\delta(\text{C}_{\text{C}=\text{O}}\text{CX})$ movement significantly contributes to Raman intensity, especially for iodine. Raman spectra of chloro and bromo esters differed in bands where $\delta(\text{HCX})$ motion contributes (Fig. 11).

3.5. Photochemical instability of ethyl 2-iodopropionate

In contrast to chloro and bromo derivatives, the iodo ester is extremely unstable. We were able to prepare only a limited amount of the ester, and with limited purity. This is because of the photochemical instability of the compound in visible light, confirmed also during attempts to measure Raman and ROA. As a result, ROA spectra of ethyl 2-iodopropionate could not be accumulated due to rapid photolysis (Fig. 12). The iodine formed by the photolysis absorbed most of the scattered light and significantly suppressed the Raman signal. The Raman spectra were acquired using a low laser power at the sample, 14 mW (Fig. 12). The stretching vibration of iodine in ethyl 2-iodopropionate 200 cm^{-1} is slightly redshifted in comparison with the vibration in ethanol and acetone (202 cm^{-1}) [37] and slightly blueshifted than that in dimethylnitrosamine (198 cm^{-1}). Even when the iodo ester was

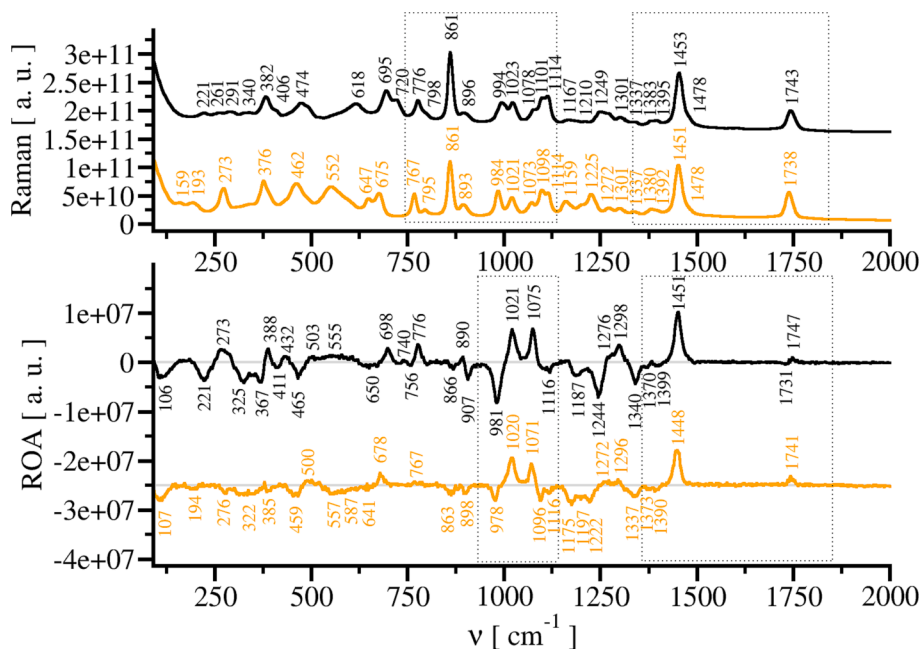


Fig. 11. Raman and ROA spectra of ethyl (2S)-chloropropionate (black) and ethyl (2S)-bromopropionate (yellow, 1.5x magnified). Quasi conserved regions are indicated by dotted rectangles. (For interpretation of the references to colour in this figure legend, the reader is referred to the web version of this article.)

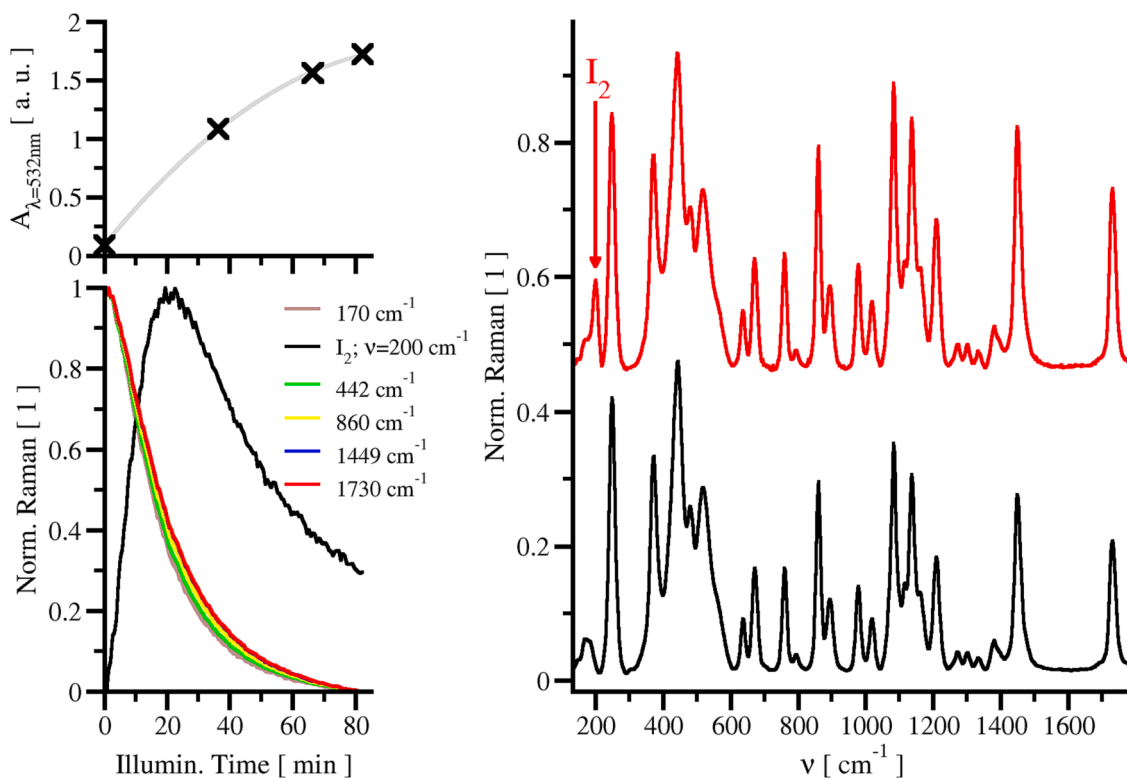


Fig. 12. Raman intensities of selected bands as dependent on time (left, the changes are due to the photolysis of ethyl 2-iodopropionate in the 532 nm laser radiation), and the spectra before (black) and after (red) measurement (right, iodine peak is indicated). (For interpretation of the references to colour in this figure legend, the reader is referred to the web version of this article.)

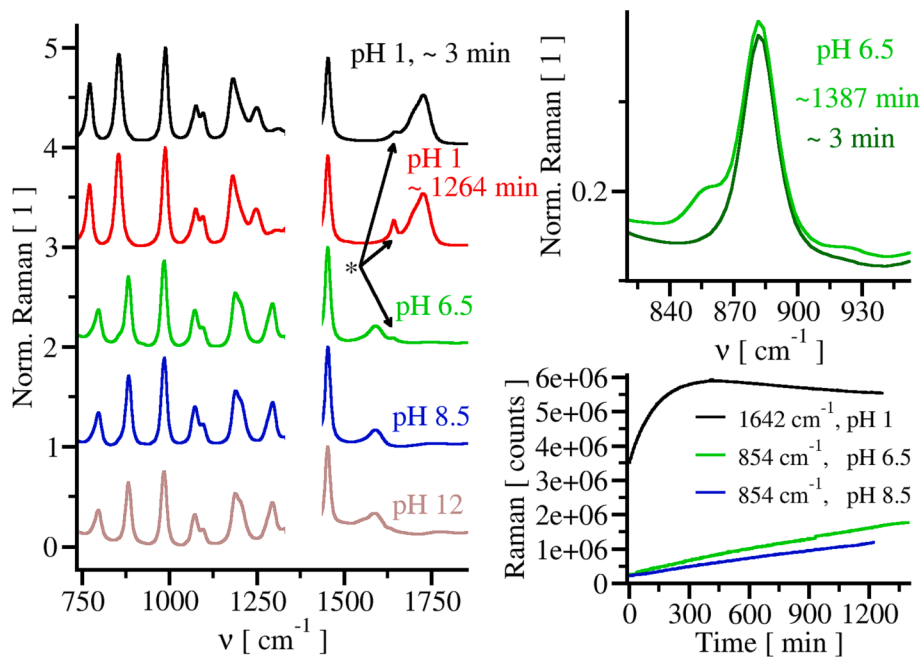


Fig. 13. Instability of 2-bromopropionic acids in water at various pH. Raman spectra were normalized in regions displayed at the left panel. * is carbonyl vibration of decomposition product at 1642 cm⁻¹. Raman spectra were deleted in region 1331 to 1434 cm⁻¹ for normalization in order to emphasized tiny changes caused by decomposition.

stored in freezer for month, the colorless liquid turned to dark brown due to the dissolved iodine.

3.6. Spectra of the haloacids measured in water solutions

As shown earlier [38–40] the acids dissociate in water. Because of the propensity to nucleophilic substitution [41], they may also

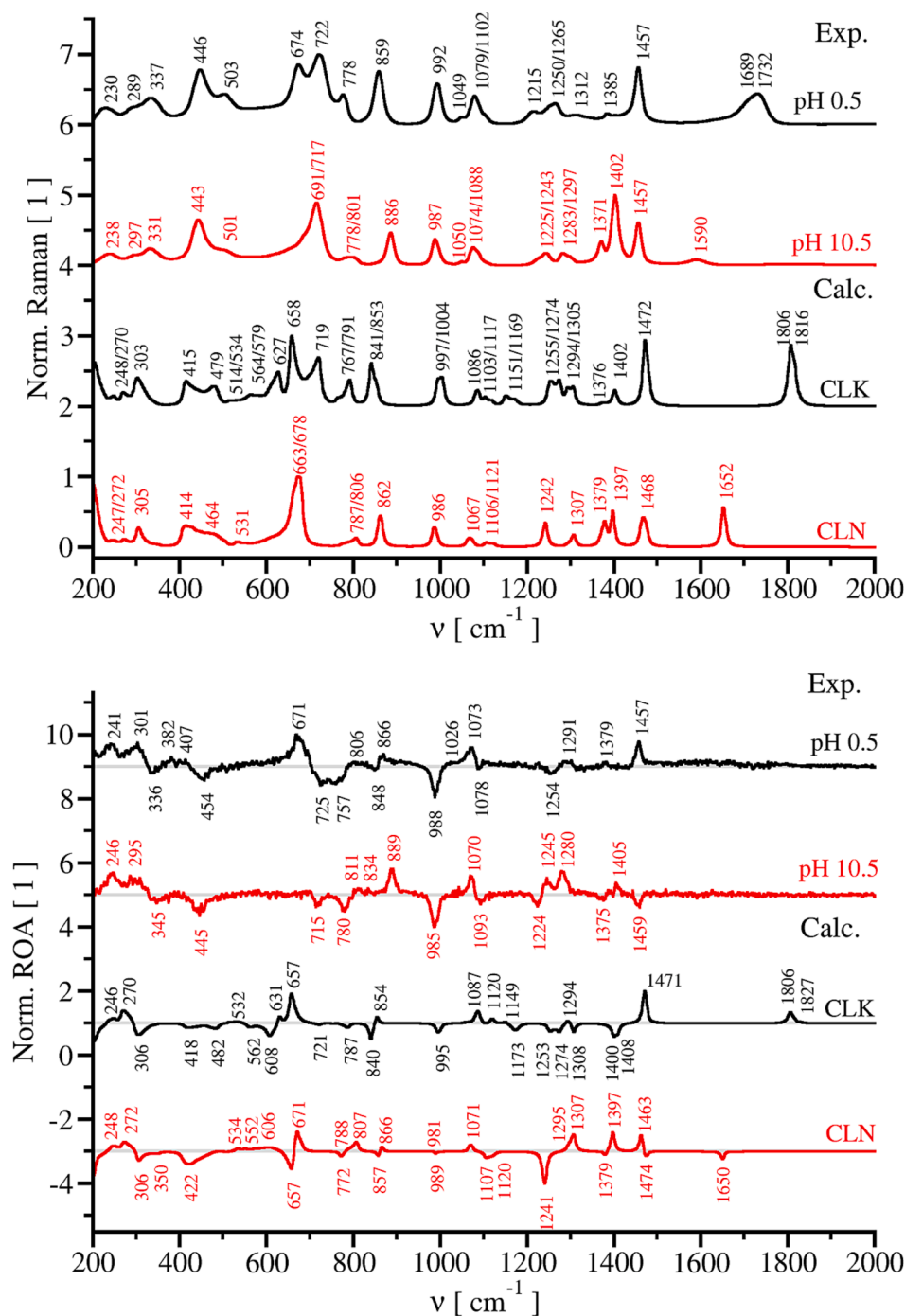


Fig. 14. Experimental and calculated Raman and ROA spectra of (2S)-chloropropionic acids (CLK) and its anion (CLN) in water. Calculated spectra are for average of 3000 conformers.

decompose. In our case, it was possible to obtain Raman and ROA spectra for chloropropionic acid only. At pH 1, 2-bromopropionic acid formed a compound with a signal at 1642 cm^{-1} (Figs. 13 and S17). In neutral pH, an impurity developed a vibration at ca 854 cm^{-1} , while basic pH 12 led to a dramatic growth of fluorescence (not shown).

Comparison of the dissociated and neutral form of 2-chloropropionic acid helps us to verify the band assignments. The main trends in the spectra were reproduced (Fig. 14). In contrast to the neat acid (Figs. 4 and 5) carbonyl ROA is not visible. The calculated carbonyl frequencies are by 117 cm^{-1} and 62 cm^{-1} higher than experiment for neutral and anionic species, respectively. Also the changes in Raman spectra within $600\text{--}900\text{ cm}^{-1}$ caused by the deprotonation are well reproduced,

including the $\nu(\text{C--Cl})$ signal at (exp) 722 cm^{-1} . The influence of deprotonation on $\delta(\text{HCH})$ and $\delta(\text{HCC})$ bands was also partially reproduced by calculation, within $1350\text{--}1500\text{ cm}^{-1}$. Bigger problems are within $1200\text{--}1350\text{ cm}^{-1}$ (mostly $\delta(\text{HCCL})$) and $400\text{--}530\text{ cm}^{-1}$ ($\delta(\text{HCCL})$ and $\nu(\text{C--Cl})$), where the theory reproduces fine Raman patterns only approximately, and even bigger inconsistencies appear in ROA (Fig. 14). Most probably, this can be attributed to inadequate conformer sampling in MD.

4. Conclusions

We have synthesized model halogen acid and their derivatives, and

studied them with molecular dynamics, Raman and ROA spectroscopy. We have shown that residual water can change both Raman and ROA spectra of studied halogenated acids. This “reversed” solvation of the water by the studied compounds caused spectral changes explicable by two mechanisms. First, the solvation led to specific organization in first solvation sphere, different from those in absence of water. Second, the water served as a base and influenced the acido-basic equilibrium. A significant decomposition of iodo ester in laser light prevented measurement of reliable ROA spectrum. The MD and DFT simulations were found suitable to explain some observed trends in spectral behavior, with some inconsistencies namely for the bromo and iodo derivatives.

CRedit authorship contribution statement

Marie Berešová: Investigation. **Jiří Bufka:** Investigation. **Martin Šafařík:** Investigation. **Petr Bouř:** Writing – review & editing, Software. **Jaroslav Šebestík:** Writing – original draft, Software, Methodology, Investigation, Formal analysis.

Declaration of Competing Interest

The authors declare the following financial interests/personal relationships which may be considered as potential competing interests: Petr Bouř reports financial support was provided by Czech Science Foundation. If there are other authors, they declare that they have no known competing financial interests or personal relationships that could have appeared to influence the work reported in this paper.

Data availability

Data will be made available on request.

Acknowledgments

This work was supported by the Czech Science Foundation (22-04669S), Research Project RVO 61388963. Computational resources were supplied by the project “e-Infrastruktura CZ” (e-INFRA CZ LM2018140) supported by the Ministry of Education, Youth and Sports of the Czech Republic. The molecular structures were visualized using program UCSF Chimera. [42]

Appendix A. Supplementary data

Supplementary data to this article can be found online at <https://doi.org/10.1016/j.saa.2024.123852>. Experimental Raman and ROA spectra of enantiomeric pairs of chloro and bromo acids and esters; tables with complete assignment of vibrational modes using automatic SW are available.

References

- X.M. Zhang, H.Q. Dou, Z.B. Zhang, W. Zhang, X.L. Zhu, J. Zhu, Fast and effective copper(0)-mediated simultaneous chain- and step-growth radical polymerization at ambient temperature, *J. Polym. Sci. A Polym. Chem.* 51 (2013) 3907–3916, <https://doi.org/10.1002/pola.26792>.
- B. Turel, S. Karatas, A. Gungor, I.E. Serhatli, Synthesis of triphenyl phosphine oxide-containing polymers via atom transfer radical polymerization, *J. Appl. Polym. Sci.* 128 (2013) 888–898, <https://doi.org/10.1002/app.38271>.
- L.T. Strover, J. Malmstrom, O. Laita, J. Reynisson, N. Aydemir, M.K. Nieuwoudt, D. E. Williams, P.R. Dunbar, M.A. Brimble, J. Trivas-Sejdic, A new precursor for conducting polymer-based brush interfaces with electroactivity in aqueous solution, *Polymer* 54 (2013) 1305–1317, <https://doi.org/10.1016/j.polymer.2012.11.083>.
- K. Qi, Q.G. Ma, E.E. Remsen, C.G. Clark, K.L. Wooley, Determination of the bioavailability of biotin conjugated onto shell cross-linked (SCK) nanoparticles, *J. Am. Chem. Soc.* 126 (2004) 6599–6607, <https://doi.org/10.1021/ja039647k>.
- Z. Wimmer, S. Vašíčková, D. Šaman, M. Romáňuk, Oxime ethers as potential juvenoids: synthesis of optical isomers, *Liebigs Ann. Chem.* 1990 (1990) 847–852, <https://doi.org/10.1002/jlac.199019901159>.
- Z. Wimmer, D. Šaman, W. Francke, Novel juvenoids of the 2-(4-hydroxybenzyl) cyclohexan-1-one series, *Helv. Chim. Acta* 77 (1994) 502–508, <https://doi.org/10.1002/hlca.19940770210>.
- V. Raghavan, C.L. Covington, P.L. Polavarapu, Specific optical rotation for the identification of the locus of solubilization of chiral molecules in achiral micelles, *J. Mol. Spec.* 350 (2018) 1–9, <https://doi.org/10.1016/j.jms.2018.05.002>.
- B. Dutta, T. Tanaka, A. Banerjee, J. Chowdhury, Conformational preferences of ethyl propionate molecule: Raman, temperature dependent FTIR spectroscopic study aided by ab initio quantum chemical and Car-Parrinello molecular dynamics simulation studies, *Chem. A Eur. J.* 117 (2013) 4838–4850, <https://doi.org/10.1021/jp404247v>.
- J. Crassous, A. Collet, The bromochlorofluoromethane saga, *Enantiomer* 5 (2000) 429–438.
- S. Gobi, E. Vass, G. Magyarfalvi, G. Tarczay, Effects of strong and weak hydrogen bond formation on VCD spectra: a case study of 2-chloropropionic acid, *PCCP* 13 (2011) 13972–13984, <https://doi.org/10.1039/c1cp20797k>.
- S. Qiu, G.N. Li, P. Wang, G.Q. Jia, Z.C. Feng, C. Li, Hydrogen bonding in homochiral dimers of hydroxyesters studied by Raman optical activity spectroscopy, *J. Raman Spect.* 43 (2012) 503–513, <https://doi.org/10.1002/jrs.3056>.
- J. Bloino, M. Biczyński, V. Barone, Anharmonic effects on vibrational spectra intensities: infrared, Raman, vibrational circular dichroism, and Raman optical activity, *Chem. A Eur. J.* 119 (2015) 11862–11874, <https://doi.org/10.1021/acs.jpca.5b10067>.
- P. Michal, R. Čelechovský, M. Dudka, J. Kapitán, M. Vůjtek, M. Berešová, J. Šebestík, K. Thangavel, P. Bouř, Vibrational optical activity of intermolecular, overtone, and combination bands: 2-chloropropionitrile and alpha-Pinene, *J. Phys. Chem. B* 123 (2019) 2147–2156, <https://doi.org/10.1021/acs.jpcc.9b00403>.
- B. Koppenhoefer, V. Schurig, (S)-2-Chloroalkanoic acids of high enantiomeric purity from (S)-2-amino acids: (S)-2-Chloropropionic acid, *Org. Synth.* 66 (1988) 151–155, <https://doi.org/10.15227/orgsyn.066.0151>.
- L. Zervas, M. Winitz, J.P. Greenstein, Studies on arginine peptides. 1. Intermediates in the synthesis of N-terminal and C-terminal arginine peptides, *J. Org. Chem.* 22 (1957) 1515–1521, <https://doi.org/10.1021/jo01362a052>.
- T.W. Baughman, J.C. Sworen, K.B. Wagener, The facile preparation of alkenyl metathesis synthons, *Tetrahedron* 60 (2004) 10943–10948, <https://doi.org/10.1016/j.tet.2004.09.021>.
- W.B. Severn, J.C. Richards, A novel approach for stereochemical analysis of 1-carboxyethyl sugar ethers by NMR spectroscopy, *J. Am. Chem. Soc.* 115 (1993) 1114–1120, <https://doi.org/10.1021/ja00056a041>.
- W. Gerrard, M.J. Richmond, Experiments on the interaction of hydroxy compounds and phosphorus and thionyl halides in the absence and in the presence of tertiary bases. Part IV, *J. Chem. Soc.* (1945) 853–857, <https://doi.org/10.1039/jr9450000853>.
- W. Gerrard, J. Kenyon, H. Phillips, The replacement of the hydroxyl group of ethyl (+)-Lactate by halogens, and the molecular dissymmetry of derivatives of ethyl lactate which contain the sulphur group, *J. Chem. Soc.* (1937) 153–158, <https://doi.org/10.1039/jr9370000153>.
- J. Kenyon, H. Phillips, H.G. Turley, Investigations on the dependence of rotatory power on chemical constitution. Part XXIV. Further experiments on the Walden inversion, *J. Chem. Soc.* 127 (1925) 399–417, <https://doi.org/10.1039/ct9252700399>.
- S.C.J. Fu, S.M. Birnbaum, J.P. Greenstein, Influence of optically active acyl groups on the enzymatic hydrolysis of N-acylated-L-amino acids, *J. Am. Chem. Soc.* 76 (1954) 6054–6058, <https://doi.org/10.1021/ja01652a057>.
- Y.J. Mei, P. Dissanayake, M.J. Allen, A new class of ligands for aqueous, lanthanide-catalyzed, enantioselective Mukaiyama aldol reactions, *J. Am. Chem. Soc.* 132 (2010) 12871–12873, <https://doi.org/10.1021/ja107197p>.
- J. Šebestík, P. Bouř, Raman optical activity of methyloxirane gas and liquid, *J. Phys. Chem. Lett.* 2 (2011) 498–502, <https://doi.org/10.1021/jz200108v>.
- J. Šebestík, M. Šafařík, P. Bouř, Ferric complexes of 3-hydroxy-4-pyridinones characterized by density functional theory and Raman and UV-vis spectroscopies, *Inorg. Chem.* 51 (2012) 4473–4481, <https://doi.org/10.1021/ic202004d>.
- M.J. Frisch, G.W. Trucks, H.B. Schlegel, G.E. Scuseria, M.A. Robb, J.R. Cheeseman, G. Scalmani, V. Barone, G.A. Petersson, H. Nakatsuji, X. Li, M. Caricato, A.V. Marenich, J. Bloino, B.G. Janesko, R. Gomperts, B. Mennucci, H.P. Hratchian, J.V. Ortiz, A.F. Izmaylov, J.L. Sonnenberg, Williams, F. Ding, F. Lipparini, F. Egidi, J. Goings, B. Peng, A. Petrone, T. Henderson, D. Ranasinghe, V.G. Zakrzewski, J. Gao, N. Rega, G. Zheng, W. Liang, M. Hada, M. Ehara, K. Toyota, R. Fukuda, J. Hasegawa, M. Ishida, T. Nakajima, Y. Honda, O. Kitao, H. Nakai, T. Vreven, K. Throssell, J.A. Montgomery Jr, J.E. Peralta, F. Ogliaro, M.J. Bearpark, J.J. Heyd, E. N. Brothers, K.N. Kudin, V.N. Staroverov, T.A. Keith, R. Kobayashi, J. Normand, K. Raghavachari, A.P. Rendell, J.C. Burant, S.S. Iyengar, J. Tomasi, M. Cossi, J.M. Millam, M. Klene, C. Adamo, R. Cammi, J.W. Ochterski, R.L. Martin, K. Morokuma, O. Farkas, J.B. Foresman, D.J. Fox, *Gaussian 16 Rev. C.01*, Wallingford, CT, 2016.
- D.A. Case, V. Babin, J.T. Berryman, R.M. Betz, Q. Cai, D.S. Cerutti, T.E. Cheatham, T.A. Darden, R.E. Duke, H. Gohlke, A.W. Goetz, S. Gusarov, N. Homeyer, P. Janowski, J. Kaus, I. Kolossváry, A. Kovalenko, T.S. Lee, S. LeGrand, T. Luchko, R. Luo, B. Madej, K.M. Merz, F. Paesani, D.R. Roe, A. Roitberg, C. Sagui, R. Salomon-Ferrer, G. Seabra, C.L. Simmerling, W. Smith, J. Swails, R.C. Walker, J. Wang, R.M. Wolf, X. Wu, P.A. Kollman, *AMBER 14*, University of California, San Francisco, 2014.
- P. Niederhäfner, M. Šafařík, J. Neburková, T.A. Keiderling, P. Bouř, J. Šebestík, Monitoring peptide tyrosine nitration by spectroscopic methods, *Amino Acids* 53 (2021) 517–532, <https://doi.org/10.1007/s00726-020-02911-7>.

- [28] J.P. Perdew, K. Burke, Y. Wang, Generalized gradient approximation for the exchange-correlation hole of a many-electron system, *Phys. Rev. B* 54 (1996) 16533–16539, <https://doi.org/10.1103/PhysRevB.54.16533>.
- [29] P. Michal, J. Kapitán, J. Kessler, P. Bouř, Low-frequency Raman optical activity provides insight into the structure of chiral liquids, *PCCP* 24 (2022) 19722–19733, <https://doi.org/10.1039/d2cp02290g>.
- [30] S. Grimme, J. Antony, S. Ehrlich, H. Krieg, A consistent and accurate ab initio parametrization of density functional dispersion correction (DFT-D) for the 94 elements H-Pu, *J. Chem. Phys.* 132 (2010) 154104, <https://doi.org/10.1063/1.3382344>.
- [31] A. Bergner, M. Dolg, W. Kuchle, H. Stoll, H. Preuss, Ab-initio energy-adjusted pseudopotentials for elements of groups 13–17, *Mol. Phys.* 80 (1993) 1431–1441, <https://doi.org/10.1080/00268979300103121>.
- [32] P. Bouř, T.A. Keiderling, Partial optimization of molecular geometry in normal coordinates and use as a tool for simulation of vibrational spectra, *J. Chem. Phys.* 117 (9) (2002) 4126–4132, <https://doi.org/10.1063/1.1498468>.
- [33] K. Ruud, A.J. Thorvaldsen, Theoretical approaches to the calculation of raman optical activity spectra, *Chirality* 21 (2009) E54–E67, <https://doi.org/10.1002/chir.20777>.
- [34] P. Bouř, J. Sopková, L. Bednářová, P. Maloň, T.A. Keiderling, Transfer of molecular property tensors in Cartesian coordinates: A new algorithm for simulation of vibrational spectra, *J. Comput. Chem.* 18 (1997) 646–659, [https://doi.org/10.1002/\(SICI\)1096-987X\(19970415\)18:5<646::AID-JCC6>3.0.CO;2-N](https://doi.org/10.1002/(SICI)1096-987X(19970415)18:5<646::AID-JCC6>3.0.CO;2-N).
- [35] S. Yamamoto, P. Bouř, Transition polarizability model of induced resonance Raman optical activity, *J. Comput. Chem.* 34 (2013) 2152–2158, <https://doi.org/10.1002/jcc.23370>.
- [36] M.E.R. Robinson, D.I. Bower, W.F. Maddams, Study of C-Cl stretching region of Raman-spectrum of PVC, *Polymer* 19 (1978) 773–784, [https://doi.org/10.1016/0032-3861\(78\)90004-6](https://doi.org/10.1016/0032-3861(78)90004-6).
- [37] P. Klaeboe, The Raman spectra of some iodine, bromine, and iodine monochloride charge-transfer coomplexes in solution, *J. Am. Chem. Soc.* 89 (1967) 3667–3676, <https://doi.org/10.1021/ja00991a001>.
- [38] P.L. Polavarapu, E.A. Donahue, K.C. Hammer, V. Raghavan, G. Shanmugam, I. Ibnusaud, D.S. Nair, C. Gopinath, D. Habel, Chiroptical spectroscopy of natural products: avoiding the aggregation effects of chiral carboxylic acids, *J. Nat. Prod.* 75 (2012) 1441–1450, <https://doi.org/10.1021/np300341z>.
- [39] P.L. Polavarapu, J.L. Johnson, V. Raghavan, G. Zając, M. Baranska, Vibrational Raman optical activity of diacetyl L-tartaric acid and corresponding surfactants: Sodium salts and shorter analogs of surfactants simplify the interpretations, *J. Raman Spectrosc.* 53 (2022) 1102–1114, <https://doi.org/10.1002/jrs.6334>.
- [40] J. Kaminský, F. Horácková, N. Biácková, T. Hubácková, O. Socha, J. Kubelka, Double hydrogen bonding dimerization propensity of aqueous hydroxy acids investigated using vibrational optical activity, *J. Phys. Chem. B* 125 (2021) 11350–11363, <https://doi.org/10.1021/acs.jpcc.1c05480>.
- [41] P. Walden, Ueber die gegenseitige Umwandlung optischer Antipoden, *Ber. Dtsch. Chem. Ges.* 29 (1896) 133–138, <https://doi.org/10.1002/cber.18960290127>.
- [42] E.F. Pettersen, T.D. Goddard, C.C. Huang, G.S. Couch, D.M. Greenblatt, E.C. Meng, T.E. Ferrin, UCSF chimera - a visualization system for exploratory research and analysis, *J. Comput. Chem.* 25 (2004) 1605–1612, <https://doi.org/10.1002/jcc.20084>.